

# Structure and luminescence of annealed nanoparticles of ZnS:Mn

A. D. Dinsmore,<sup>a)</sup> D. S. Hsu, S. B. Qadri, J. O. Cross,<sup>b)</sup> T. A. Kennedy, H. F. Gray, and B. R. Ratna

Naval Research Laboratory, 4555 Overlook Avenue, SW, Washington, D.C. 20375

(Received 11 April 2000; accepted for publication 3 August 2000)

Structural and light-emitting properties of nanoparticles of ZnS:Mn annealed in vacuum at temperatures up to 525 °C are presented. Annealing the 3.5 nm particles at temperatures up to 350 °C caused growth of some particles without substantial change in the luminescence or ZnS lattice. After annealing at 400–525 °C, the high-temperature wurtzite phase of ZnS appeared, accompanied by an increase of the average particle diameter to approximately 100 nm and a rearrangement of the Mn ions. Dramatic increase in cathodoluminescence emission was also observed and is compared to the structural information obtained from electron microscopy, x-ray diffraction, x-ray absorption fine structure, and electron paramagnetic resonance measurements.

© 2000 American Institute of Physics. [S0021-8979(00)06421-5]

## I. INTRODUCTION

A great deal of attention has been devoted to the novel properties of nanometer-sized particles. When the particle size is in the nm range, the electronic properties are perturbed by quantum-mechanical confinement effects and the thermodynamics are heavily influenced by surface effects. For example, semiconductor nanoparticles exhibit size-dependent electronic band gap energies<sup>1,2</sup> melting temperatures,<sup>3,4</sup> and solid-solid phase transition temperatures<sup>5,6</sup> and pressures.<sup>7,8</sup> In addition to their fundamental interest, *doped* semiconductor nanoparticles have tremendous potential for use in light-emitting applications. Examples include Y<sub>2</sub>O<sub>3</sub>:Tb,<sup>9,10</sup> Y<sub>2</sub>O<sub>3</sub>:Eu,<sup>11–13</sup> LaPO<sub>4</sub>:Eu, Ce and Tb,<sup>14</sup> CdS:Mn,<sup>15</sup> CdSe:Mn,<sup>16</sup> ZnS:Cu,<sup>17</sup> ZnS:Tb,<sup>18</sup> and ZnS:Mn,<sup>19–32</sup> which is the focus of this article. The photoluminescent efficiency of nanoparticles may be higher than bulk ZnS:Mn<sup>20,26</sup> and a particle-size-dependent increase in the electronic band gap energy allows control of the excitation spectrum. In addition, bright cathodoluminescence was recently observed from ZnS:Mn nanoparticles after they were annealed at 525 °C.<sup>6</sup> A remarkable 600° reduction in the zincblende-to-wurtzite transition temperature was also reported.<sup>5,6</sup> The use of nanoparticles as precursors, therefore, enables excellent luminescent properties after processing at temperatures hundreds of degrees lower than those typically used for bulk materials. To date, however, there has been a shortage of systematic studies of how the structural and optical properties change when these nanoparticles are annealed.

In this article, we describe experimental studies of the structure and luminescence of nanoparticles of ZnS doped with Mn, with emphasis on the changes that occur after an-

nealing the particles at various temperatures. Specifically, we report on the properties of nanoparticles as-made (i.e., unannealed) and after annealing in vacuum at 300, 350, 400, and 525 °C. Results of x-ray diffraction, transmission electron microscopy (TEM), extended x-ray absorption fine structure (EXAFS), electron paramagnetic resonance (EPR), and photoluminescence (PL) and cathodoluminescence (CL) measurements will be presented. After annealing at the higher temperatures, we observed increase of the crystallite and particle sizes, relaxation of strain and a phase change in the ZnS lattice, and changes in the environment around the Mn ions. We will discuss how these structural changes relate to changes in the luminescent properties.

## II. EXPERIMENTAL PROCEDURES

The particles were synthesized using the bicontinuous cubic phase of a surfactant–water mixture as a template to control particle size.<sup>26,33,34</sup> First, an aqueous solution of 0.1 M ZnCl<sub>2</sub> (99.999%, Aldrich Chemical Co., Milwaukee, WI) and 7.0 × 10<sup>-4</sup> M MnCl<sub>2</sub> · 4H<sub>2</sub>O (99.99%, Aldrich) was made. The molar ratio of Mn to Zn was 0.7%. The aqueous solution was mixed with a surfactant, sodium dioctyl sulfosuccinate (AOT, 99%, Sigma Chemical Co., St. Louis, MO), in the ratio 40 wt % aqueous solution and 60 wt % AOT. After 2 of occasional stirring, a transparent, viscous paste formed. The paste was injected through 3 mL syringes into a solution of 0.2 M Na<sub>2</sub>S · 9H<sub>2</sub>O (99.3%, Sigma) and 0.1 M NaCl (99+%, Aldrich). After 3 h, the aqueous supernatant was discarded and the sample was rinsed in water by centrifugation, then rinsed in methanol.

Unless otherwise stated, we applied an inorganic “capping” layer on the surface of the nanoparticles. These particles will henceforth be designated “ZnS:Mn/ZnO.” As will be discussed below, this step substantially increased the CL. After the first methanol rinse, the particles were suspended in water containing a measured amount of ZnCl<sub>2</sub> (1/4 or 1/10 the amount of ZnCl<sub>2</sub> used in the primary synthesis step). Drops of 0.5 M NaOH were then added to raise the pH to approximately 10, at which point Zn(OH)<sub>x</sub> or ZnO pre-

<sup>a)</sup> Author to whom correspondence should be addressed; Present address: Harvard University, Division of Engineering and Applied Sciences, 9 Oxford Street, Cambridge, MA 02138; electronic mail: dinsmore@deas.harvard.edu

<sup>b)</sup> Present address: Argonne National Laboratory, Building 435E, 9700 South Cass Avenue, Argonne, IL 60439.

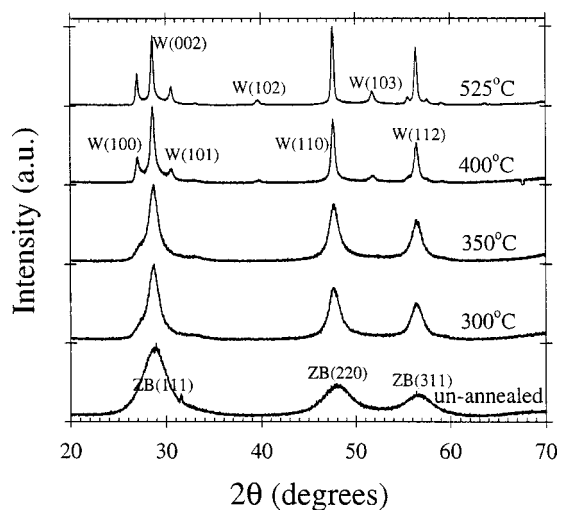


FIG. 1. XRD spectra ( $\theta/2\theta$  scan) of ZnS:Mn/ZnO nanoparticles after annealing at various temperatures in vacuum. Peak assignments for zincblende (ZB) and wurtzite (W) structures are shown. After annealing at 400 and 525 °C, a coexistence of the two phases is observed. Lattice parameters and average crystallite sizes extracted from these spectra are listed in Table I.

precipitated at the particles' surfaces. For some samples,  $\text{MgCl}_2$  was substituted for the  $\text{ZnCl}_2$  during the capping procedure. After approximately 2 min, samples were rinsed in water, then in methanol, then in dichloromethane, and finally dried in a vacuum.

The annealing was done at high vacuum ( $10^{-7}$  Torr) in a zirconium oxide crucible. The temperature was raised to 200 °C, then left for several hours, then increased at 20°/m. The maximum temperature (up to 525 °C) was held for 35 min, after which the sample was cooled to room temperature at 15°–20°/m, and finally removed from vacuum. The annealed, ZnO-capped powders were light tan in color. The particles with no inorganic capping or with MgO capping were dark gray or black in color after annealing.

To measure the structure of the ZnS host and the sizes of the crystallites before and after annealing, x-ray diffraction measurements were done with a Rigaku two-circle diffractometer using Cu  $K\alpha$  radiation. The average crystallite diameter of each sample was inferred from the peak widths using the Scherrer equation (as in Ref. 34), taking the average of the results from the most prominent (111), (200), and (311) peaks. TEM (200 kV Hitachi 8100) was used to study the particle size and morphology. Each TEM sample was prepared by suspending the ZnS:Mn powder in methanol and evaporating a droplet onto a carbon-coated copper grid.

EPR measurements were done with a Bruker ESP300 at 9.5 GHz and a Varian E109Q at 35 GHz. Dry powders were mounted in 3 mm glass tubes, as was done previously.<sup>35</sup> The EXAFS measurements were performed at the National Synchrotron Light Source beamline X23B. A fixed-exit double-crystal Si(111) monochromator was used for scanning the incident energy and mechanically bent Pt-coated Si mirrors before and after the monochromator were used for focusing and harmonic rejection. The data were collected in fluorescence mode with an argon-gas ionization chamber. A 15  $\mu\text{m}$  thick vanadium foil was used to filter out the elastic scatter-

TABLE I. ZnS crystal structures and sizes inferred from the XRD spectra. There was a tetragonal distortion of the zincblende lattice in samples annealed to 350 °C. Coexistence of zincblende and wurtzite was observed after annealing at 400 and 525 °C. The standard bulk ZnS lattice parameters are  $a = 5.405$  Å for zincblende and  $a = 3.82098$  Å,  $c = 6.2573$  Å for wurtzite.

Anneal temperature	ZnS phase (ref. amount)	Lattice parameters (specific volume)	Average crystallite diameter (Å)
Room. temp. (unannealed)	zincblende	$a = 5.409 \pm 0.004$ Å $c = 5.340 \pm 0.008$ Å ( $156.2 \pm 0.3$ Å <sup>3</sup> )	35
300 °C	zincblende	$a = 5.404 \pm 0.012$ Å $c = 5.377 \pm 0.027$ Å ( $157.0 \pm 0.7$ Å <sup>3</sup> )	60
350 °C	zincblende	$a = 5.401 \pm 0.002$ Å $c = 5.379 \pm 0.005$ Å ( $156.9 \pm 0.2$ Å <sup>3</sup> )	84
400 °C	zincblende (81%) wurtzite (19%)	$a = 5.399$ Å $a = 3.818 \pm 0.005$ Å $c = 6.25 \pm 0.01$ Å	171
525 °C	zincblende (71%) wurtzite (29%)	$a = 5.405$ Å $a = 3.822 \pm 0.002$ Å $c = 6.253 \pm 0.005$ Å	160

ing background and tungsten Soller slits with a 2.5 in. point focus were used to block secondary scattering and fluorescence from the filter. The dry powder samples were packed into a 1 mm thick by 8 mm diam pocket under 3  $\mu\text{m}$  thick Mylar film and all measurements were made at room temperature. The samples were spun continuously at approximately 1000 rpm during measurement. Some discoloration of the samples was observed after exposure to the x-ray beam. Background subtraction and fitting were done with the UWXAFA analysis package.<sup>36</sup> Theoretical phases were calculated using FEFF 7 and fits of theory to data were performed in real ( $R$ ) space. Data were fit with  $k^2$  weighting over a range of 3–11 Å<sup>-1</sup> and uncertainties were determined from a reduced  $\chi^2$ . The amplitude factor was normalized by fitting the theoretical calculations to a Mn-doped ZnS standard, which was assumed to have four sulfur neighbors around each Mn ion.

PL measurements were obtained by suspending the particles in methanol or water in plastic or quartz cuvetts. A spectrofluorometer (SLM Aminco 8100 A) was used to probe excitation and emission spectra with wavelengths between 300 and 800 nm with 4 nm resolution. CL measurements were performed in vacuum ( $2 \times 10^{-7}$  Torr) on powder patches approximately 1 cm in diameter and 0.5–1 mm thick on indium–tin–oxide coated glass plates (for details, see Ref. 6). The electron acceleration voltages ranged from 500 to 3500 V and a bias voltage of 150 V was applied to the plate to recapture secondary electrons. The electron-beam voltage is the 150 V bias plus the gun voltage (hence, 650–3650 V). Emission spectra and luminance were measured using a calibrated Minolta CS-1000 spectroradiometer (di-

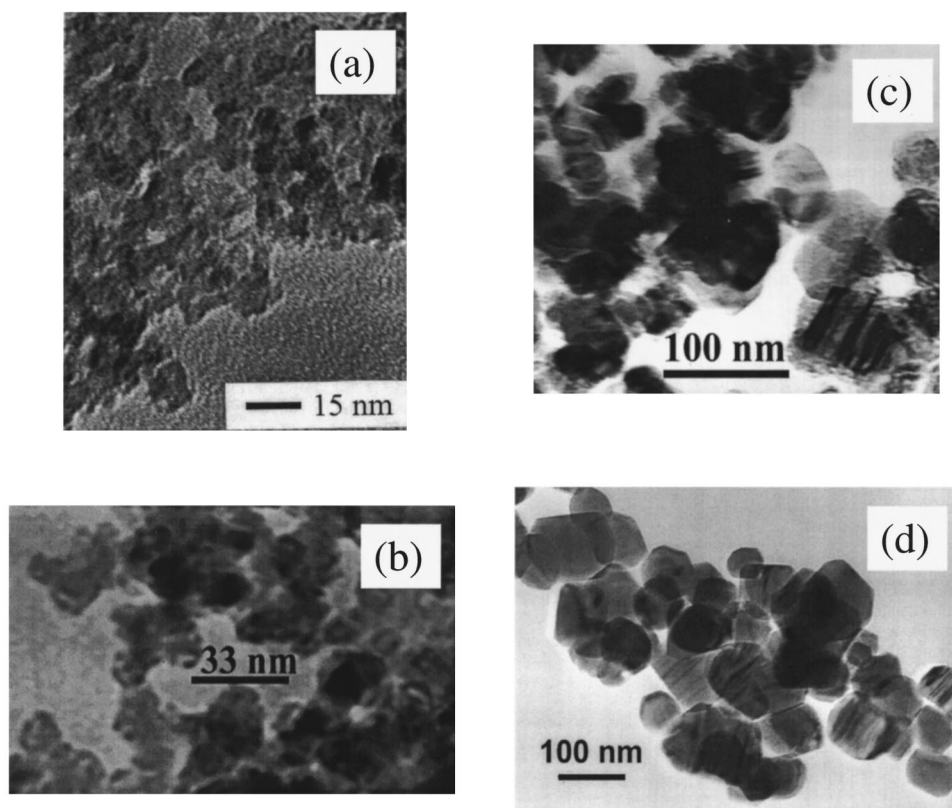


FIG. 2. TEMs of nanoparticles of ZnS:Mn/ZnO. The particles are shown after synthesis (a) and after annealing at 300 °C (b); at 400 °C (c); and at 525 °C (d). At the higher temperatures, the particles grow in size and become faceted. Samples (a)–(b) are zincblende, while (c) and (d) exhibit zincblende and wurtzite structures (inferred from XRD).

ameter of detected spot: 0.3 cm). In every case, the emission from the nanoparticles was compared to the emission from a similar-sized powder patch of a ZnS:Mn (0.5%) phosphor made by the Sarnoff Corporation (code number N826-85, Sarnoff Corp., Princeton, NJ).

### III. RESULTS

#### A. Structure, morphology, and thermodynamics

In this section, we present measurements of the structure and morphology of the particles. All of the samples discussed in this section were the ZnO-capped particles (ZnS:Mn/ZnO). We divided one sample into portions that were annealed in vacuum at temperatures of 300, 350, 400, and 525 °C. X-ray diffraction (XRD) was used to determine the ZnS crystal structure, lattice parameters, and average crystallite size. Diffraction spectra are presented in Fig. 1 and the inferred structural parameters are listed in Table I. TEM was used to determine the particle sizes and morphology. TEM images are presented in Fig. 2.

The unannealed nanoparticles exhibited the zincblende ZnS structure, which is the stable phase for room-temperature bulk ZnS. Unlike the bulk material, however, the unit cell was tetragonally distorted: the smaller parameter ( $C = 5.340 \pm 0.008 \text{ \AA}$ ) was compressed by 1.2% compared to the bulk lattice parameter, 5.405 Å.<sup>37</sup> A larger 2% lattice compression and tetragonal distortion was recently reported in *undoped* ZnS nanoparticles made using the same process.<sup>5</sup> Lattice compression and dilation have also been observed in nanoparticles of other materials, such as CdS (Ref. 3) and Pd,<sup>38</sup> and was predicted in 1930 by Lennard-Jones, who

summed the interatomic forces within a small particle.<sup>39</sup> The shifted lattice parameter does not appear to change the  $\text{Mn}^{2+}$  emission spectrum (see Sec. III).

The unannealed crystallite size (inferred from XRD) was approximately 3.5 nm, with some size variation ( $\sim 0.5$  nm) from sample to sample. Figure 2(a) shows a TEM micrograph of this sample. The particle diameter (inferred from TEM) is approximately 4 nm, slightly larger than the crystallite size. Possibly there was ZnO and/or surfactant on the particles' surfaces which made them appear larger in the TEM. Earlier high-resolution TEM studies of undoped ZnS nanoparticles synthesized using the present technique indicated that the particles are monocrystalline, highly monodisperse in size ( $\pm 7\%$ ), and slightly anisotropic in shape.<sup>5</sup>

Annealing the particles at temperatures of 300 and 350 °C had little or no effect on the lattice parameters, but increased the average crystallite sizes to 6.0 and 8.4 nm, respectively. TEM of these samples showed that the particle size distribution became bidisperse: particles approximately 11 nm in diameter [see Fig. 2(b)] were seen along with the majority of the approximately 4 nm particles.

The wurtzite structure appeared in samples that were annealed at 400 and 525 °C. The lattice parameters of the coexisting wurtzite and zincblende phases agreed with the tabulated values for bulk ZnS (see Table I).<sup>37</sup> We recently reported similar results for undoped ZnS nanoparticles.<sup>5</sup> The wurtzite (100) and (101) peaks are clearly visible next to the zincblende (111) peak in Fig. 1. Even in the 300 and 350 °C samples, there is a faint suggestion of the wurtzite (100) and (101) peaks. It is possible, therefore, that the zincblende-to-wurtzite transition occurs at temperatures as low as 300 °C.

The relative amounts of the zincblende and wurtzite phases were obtained by fitting them to all of the peaks in the x-ray spectrum and are listed in Table I. In the ten samples that were annealed at 525 °C, the fraction of material that formed the wurtzite phase ranged from 20% to 100%. The range of values may reflect subtle variations in particle size distributions or heating rate from sample to sample. To see whether the low pressure of the vacuum chamber affected the phase transition temperature, we also heated a sample to 520 °C under flowing nitrogen. XRD from the resulting powder indicated equal amounts of the zincblende and wurtzite phases. Hence the reduced zincblende-to-wurtzite transition temperature is not a result of low pressure.

We thus find that the zincblende-to-wurtzite phase transition temperature is depressed at least 600 °C below the bulk phase transition temperature of 1020 °C.<sup>40</sup> Commercial phosphors are often fired to temperatures near or in excess of 1000 °C in order to maximize luminance, which is often greater for the high-temperature phase.<sup>41</sup> A potential advantage of using nanoparticles of ZnS, therefore, is that the high-temperature phase can be attained by heating to relatively low temperatures (e.g., 400–500 °C). Aside from the possibility of reduced cost, potential advantages include the annealing of particles directly onto glass screens, which typically deform at temperatures above 600 °C.

The average crystallite sizes (from x rays) of the 400 and 525 °C samples were 17 and 16 nm, respectively, dramatically larger than the single-phase samples annealed at 350 °C. TEM indicated that, after annealing at 400 °C [Fig. 2(c)], the particle diameters increased dramatically to 30–70 nm. Facets were clearly visible in the particle shape. Finally, after annealing at 525 °C [Fig. 2(d)], the average particle diameter was approximately 100 nm. The particles had increased their volume by a factor of order 10<sup>4</sup>, yet the sample consisted of discrete particles.

Comparing the TEM results to the XRD results, we find that after annealing at temperatures up to 350 °C, a fraction of the particles grew and the average crystallite size increased from 3.5 to 8.4 nm. There was a tetragonal distortion of the ZnS lattice. Above 400 °C, the phase transition from zincblende to wurtzite ZnS was accompanied by a dramatic growth of all of the particles (to average diameter of 100 nm), the formation of facets, and relaxation of the lattice distortion.

Unannealed particles capped with ZnO exhibited no XRD from crystalline ZnO, indicating that the ZnO is very thin and/or amorphous. After annealing at 525 °C, the amount of crystalline ZnO appearing in ZnO-capped samples ranged from 0% to approximately 20%. Possibly, some of the ZnO from the cap layer formed very thin or amorphous layers between the ZnS domains during the annealing process. Careful inspection of the CL efficiency versus electron-beam voltage, however, suggested that the thickness of a surface oxide layer (if any) was comparable to that of the commercial phosphor.<sup>6</sup> Particles that were not capped with ZnO turned dark gray after annealing.

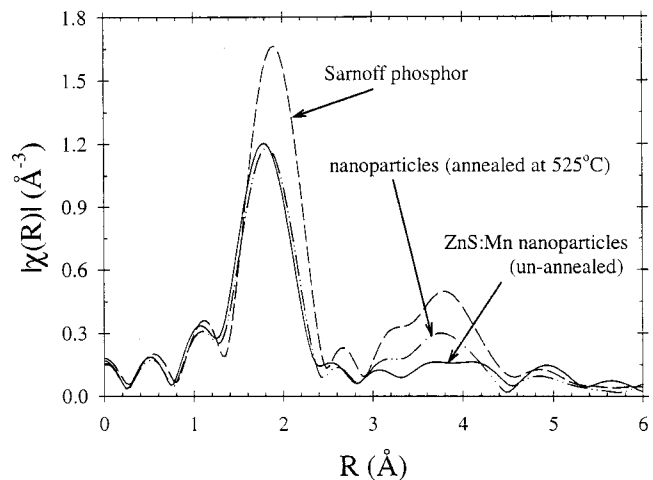


FIG. 3. EXAFS spectra of the ZnS:Mn/ZnO samples. Unannealed nanoparticles are represented by the solid curve, particles annealed at 525 °C by the dot-dashed curve, and the Sarnoff material by the dashed curve. Mn–S distances and coordination numbers obtained by fitting to these data are listed in Table II.

## B. Distribution of the Mn ions

To determine the distribution of the Mn ions within the ZnS lattice, we used EXAFS and EPR measurements. These techniques showed significant changes in the Mn distribution upon annealing the samples. The samples were the same ZnS:Mn/ZnO as in the above section.

Three *R*-space EXAFS spectra, from the unannealed and annealed nanoparticles, and from the Sarnoff (“bulk”) material, are plotted in Fig. 3. The average crystallite size of the Sarnoff material (inferred from XRD) was 32 nm, the structure was wurtzite, and the average particle size was 4 ± 1 μm.

The two peaks in the *R*-space data correspond to the nearest neighbor S and next nearest neighbor Zn around the Mn atoms. The measured spectra are consistent with Mn<sup>2+</sup> substituting for Zn<sup>2+</sup> in the lattice. Table II shows the Mn–S bond lengths and the number of S neighbors obtained by fitting the EXAFS spectra. The Mn–S bond length of 2.394 ± 0.002 Å observed for the as-grown nanoparticles is 1.4% ± 0.2% smaller than the 2.428 ± 0.004 Å for the Sarnoff bulk standard. A particle-size-dependent reduction in bond length was previously observed in monocrystalline ZnS:Mn nanoparticles.<sup>42</sup> This observation is consistent with the reduced lattice *c* parameter inferred from the x-ray diffraction spectra. Upon annealing the particles at 525 °C, the Mn–S

TABLE II. Bond lengths and coordination numbers around the Mn ions, obtained by fitting to the EXAFS spectra. The number of nearest neighbors (*S*) was set to four for the Sarnoff standard phosphor.

	Unannealed nanoparticles	Nanoparticles annealed at 525 °C	Sarnoff (“bulk” standard)
Mn–S distance	2.394 ± 0.002 Å	2.413 ± 0.002 Å	2.428 ± 0.004 Å
Number of nearest neighbors	3.73 ± 0.12	3.78 ± 0.12	4

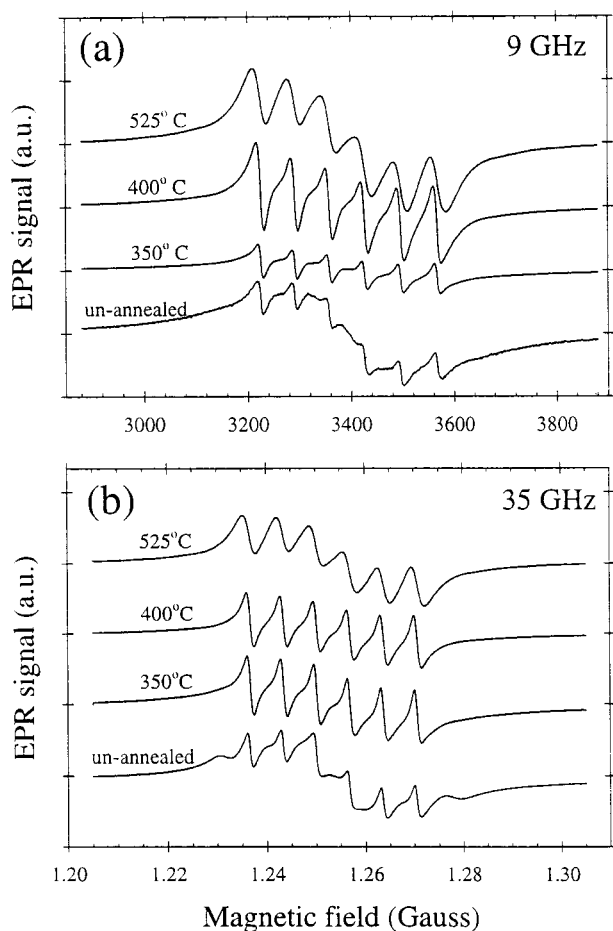


FIG. 4. EPR spectra of the ZnS:Mn/ZnO nanoparticles. Spectra are taken at 9 GHz (a) and at 35 GHz (b) before annealing and after annealing at various temperatures in vacuum.

bond length approached the bulk value, increasing to  $2.413 \pm 0.002 \text{ \AA}$ , or  $0.6\% \pm 0.2\%$  smaller than the standard.

In each of the nanoparticle EXAFS spectra, the amplitude of the first peak, which corresponds to the number of near-neighbor S around the Mn atoms, is reduced compared to that of the bulk standard. Assuming four S neighbors around the Mn in the standard, the number of S neighbors in the unannealed and annealed nanoparticles was determined to be 3.73 and 3.78, respectively (see Table II). Similar results have been reported previously.<sup>42</sup> The width of these peaks is consistent with a single bond length, so it is unlikely that the reduced number of S neighbors is caused by disorder in the first shell. It is not determined, however, whether the reduction in coordination number is due to vacancies in the lattice or to the proximity of the Mn cations to the nanoparticle surface. The magnitude of the second peak (near  $3.8 \text{ \AA}$ ) indicates that the number of second-nearest neighbors (Zn) was also smaller in the as-made nanoparticles. Similar results for nanoparticles of similar size were reported previously.<sup>42</sup> Annealing at  $525 \text{ }^\circ\text{C}$  improved the ordering, but the peak was still smaller than in the Sarnoff material.

EPR spectra measured at 9 and 35 GHz are shown in Fig. 4. All of these spectra are consistent with  $\text{Mn}^{2+}$  residing in the  $\text{Zn}^{2+}$  sites of the lattice. Visible in the spectra are the

six peaks due to hyperfine interactions between the  $d$  electrons and the spin-5/2 nucleus of the Mn.

The unannealed sample exhibits a distinct six-line spectrum having a larger hyperfine splitting with peaks evident near the edges of the 35 GHz data. These peaks are not resolved in the 9 GHz spectrum. These effects have been observed previously in samples prepared by reaction of diethylzinc and diethylmanganese with hydrogen sulfide in toluene.<sup>35</sup> Here, as in the previous study, the frequency dependence of the resolution of these peaks allows an estimate of the strength of the axial field that is responsible for them. The relatively large magnitude of this axial field and its dependence on molecular groups capping the nanoparticles led to its being attributed to the proximity of the Mn ions to the particle surface.<sup>24,35</sup> Similar surface-related effects were seen in CdS:Mn.<sup>15</sup> These perturbations to the environment around the Mn ions in the unannealed samples do not appear to affect the PL emission spectrum, which will be discussed below.

After annealing the samples at  $350 \text{ }^\circ\text{C}$ , the spectrum with larger hyperfine splitting has disappeared, leaving the spectrum from cubic (or nearly cubic) sites. The sites with a strong axial field, which may be due to the particle surface, have mostly or entirely vanished. The XRD and TEM studies indicate a growth of the particle and crystallite sizes, so the change in the EPR structure may be due to the greater distance between the Mn ions and the surfaces of the (larger) crystalline domains or particles.

The broad background peak and the widths of the six hyperfine peaks, most visible in the 9 GHz spectra, are likely due to magnetic interactions among the Mn ions. We have observed that these features become more prominent when the anneal temperature is raised from  $400$  to  $525 \text{ }^\circ\text{C}$ . As the particles coalesce, the axial fields decrease but the Mn–Mn interactions become stronger due to a decrease in the average separation between Mn ions.

### C. Luminescence

In this section, we report on the results of PL and CL measurements. Although we will focus on the CL properties (which are more relevant for field-emission display applications), the PL properties are reported both to understand the fundamental properties of the particles and for comparison to the CL data.

#### 1. Photoluminescence

The photoluminescent emission and excitation spectra of the unannealed ZnS:Mn nanoparticles suspended in methanol are shown in Fig. 5. The particles were excited with photons of energy greater than the ZnS band gap energy. The yellow–orange emission, with a peak wavelength ( $\lambda_{\text{peak}}^{\text{em}}$ ) of  $588 \text{ nm}$ , is attributed to transitions involving the  $d$  electrons of the  $\text{Mn}^{2+}$  ions.<sup>43,44</sup> Emission spectra of the uncapped and the ZnO-capped nanoparticles are very similar. Figure 5 also shows the emission spectrum of “bulk” ZnS:Mn suspended in water. This sample was prepared by mixing  $\text{Na}_2\text{S}$  with  $\text{ZnCl}_2$  and  $\text{MnCl}_2$  in water (in the same ratios as were used to make nanoparticles) *without* the surfactant to restrict the particle size. XRD from the precipitate revealed the presence of

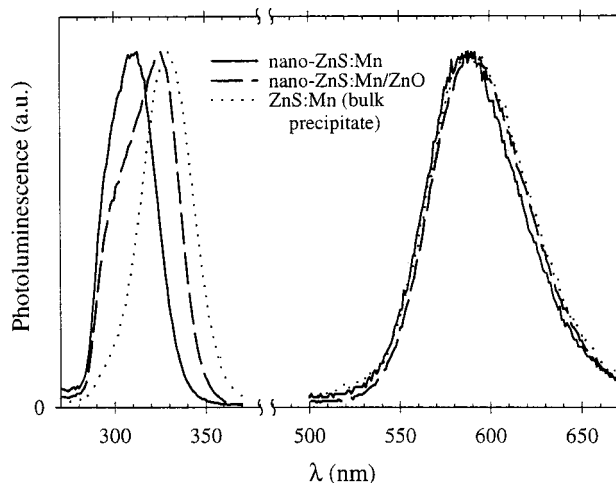


FIG. 5. PL excitation and emission spectra (spectral irradiance) of unannealed ZnS:Mn samples. Three samples are shown: the uncapped nanoparticles (solid curves), ZnO-capped nanoparticles (dashed curves), and the bulk material (dotted curves). For the excitation spectra (left), the emission at 590 nm was monitored. For the emission spectra (right), the excitation wavelength was chosen from the peak of the corresponding excitation spectrum. The height of each peak is arbitrarily scaled.

zincblende ZnS. The emission spectrum from this bulk precipitate ( $\lambda_{\text{peak}}^{\text{em}} = 590$  nm) was very similar to that of the nanoparticles. Hence, we conclude that *the particle size does not significantly affect the emission wavelength*, despite the tetragonal distortion of the ZnS lattice and the reduction of the Mn–S bond length.

The emission of the unannealed nanoparticles is, however, slightly redshifted compared to the Sarnoff phosphor ( $\lambda_{\text{peak}}^{\text{em}} = 582$  nm; not shown in Fig. 5).<sup>26</sup> Although previous authors have attributed this redshift to the small size of the nanoparticles,<sup>23,45</sup> we suggest that it might arise instead from the different crystal structures—wurtzite for the Sarnoff phosphor and zincblende for the nanoparticles. Previous experiments have shown that emission of Mn in zincblende ZnS is slightly redder than Mn in wurtzite.<sup>43</sup>

The PL excitation spectrum of the nanoparticles exhibits a dramatic blueshift compared to the bulk precipitate (see Fig. 5). The peak wavelength ( $\lambda_{\text{peak}}^{\text{ex}}$ ) of the bulk precipitate was 330 nm;  $\lambda_{\text{peak}}^{\text{ex}}$  of the nanoparticles ranged from sample to sample from approximately 310–315 nm. This blueshift was reported previously<sup>19,20,22,26–28,30</sup> and attributed to the quantum confinement effect, which increases the band-gap energy.<sup>46</sup> The distortion of the ZnS lattice might also play a role in the shift of the electronic band structure. Over time, the excitation spectrum of the uncapped particles shifted toward the red (to the bulk value), presumably due to coarsening or aggregation of the particles. Two h after synthesis, the excitation peak was at 310 nm; after 50 h, the peak shifted to 315 nm. The emission spectrum did not change during this time. The ZnO-capped particles are also blueshifted compared to the bulk material, but by a smaller amount than the uncapped particles. The smaller blueshift may be a result of the slightly larger total size of the capped particles, which would lead to less quantum confinement.

The quantum efficiency of the unannealed nanoparticles made with the present technique was previously found to be

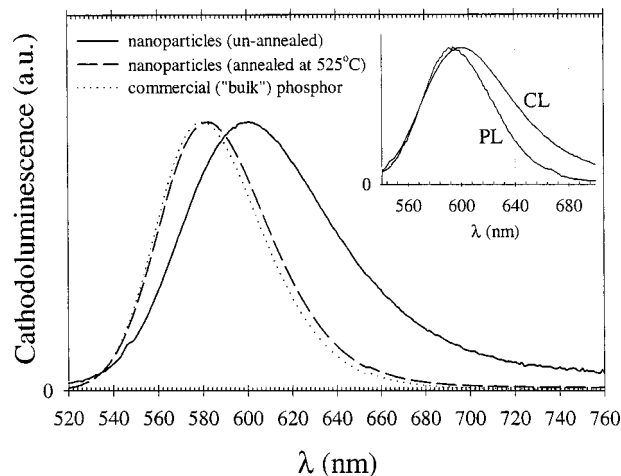


FIG. 6. CL spectra (spectral irradiance) of ZnS:Mn/ZnO samples. The unannealed nanoparticles (solid curve), annealed nanophosphors (dashed curve), and the Sarnoff phosphor (dotted curve) are shown. The electron acceleration voltage was 650 V and the current was 24  $\mu\text{A}$  (120  $\mu\text{A}/\text{cm}^2$ ). (Inset) Comparison of the PL and CL spectra of the unannealed nanoparticles.

as high as 25%.<sup>26</sup> When the material is annealed at 525 °C, however, the PL is too dim for accurate measurements. The poor efficiency may be a result of impurities in the material, which are evident from the tan color of the powder.

## 2. Cathodoluminescence

The CL spectrum of the unannealed ZnS:Mn/ZnO nanoparticles is shown in Fig. 6. The emission was substantially redshifted and broadened compared to the PL spectra of the same sample (inset of Fig. 6). The redshift of the CL decreased as the electron voltage was increased. In addition, we found that during electron-beam excitation, the emission intensity degraded noticeably within minutes. The redshift and broadening, the change in spectrum with voltage, and the degradation with time, were not observed in the annealed samples. To determine whether these properties are inherent to the Mn sites in nanoparticles, we studied the emission from powders containing a mixture of the nanoparticles with a commercial, blue-emitting ZnS:Ag phosphor. On a single plate, we prepared a patch of pure ZnS:Ag phosphor (type 1330, lot BT9613, Osram Sylvania, Towanda, PA) and a patch containing a mixture of the nano-ZnS:Mn (48 wt %) and the ZnS:Ag (52 wt %) Figure 7 shows the CL emission spectra from both of these samples. The ZnS:Ag patch exhibited a single blue CL (peak wavelength at 449 nm, independent of voltages in the range of 0.5–2.5 kV), while the mixed patch exhibited two peaks, one due to the ZnS:Ag (at 451 nm), the other due to the ZnS:Mn (at 600 nm; see inset of Fig. 7). There was negligible overlap of the blue and orange peaks. We found that the blue ZnS:Ag emission was redshifted and broadened when in the presence of the ZnS:Mn nanoparticles.

We suspect that charging of the unannealed nanoparticles during excitation is responsible for the redshift and broadening, the change in spectrum with voltage, and the degradation with time. Additional washing of the nano-ZnS:Mn in dichloromethane did not affect the emission. Fur-

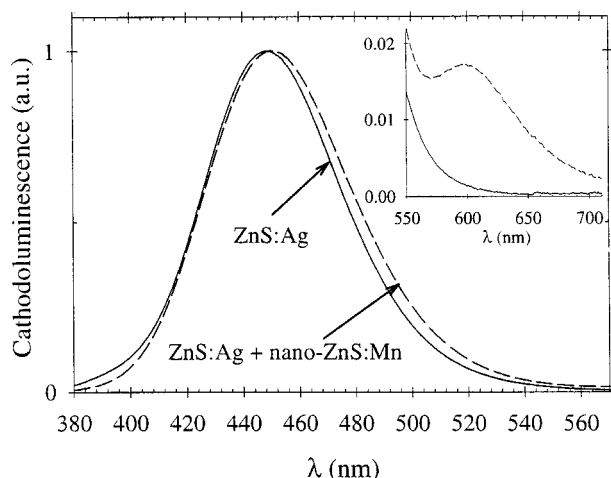


FIG. 7. Plot of the CL spectra (spectral irradiance) of the commercial ZnS:Ag phosphor (solid curve) and of a mixture of the ZnS:Ag with the unannealed ZnS:Mn/ZnO nanoparticles (dashed curve). The spectrum of the mixed powder has been multiplied by a factor of 19 to facilitate comparison. The redshift of the blue emission from the Ag centers may be due to charging of the sample because of the nanoparticles. (Inset) same data and same scaling, but a different range of  $\lambda$ , showing the Mn emission from the mixed powder.

thermore, rinsing the ZnS:Ag in an aqueous solution of AOT surfactant, then in methanol, and in dichloromethane (as was done when synthesizing the nanoparticles) before preparation of the powder patch did not induce any redshift in the ZnS:Ag emission. The charging appears, therefore, not to be a result of surfactant residue. It might instead be a result of the very small particle size. A redshift and broadening of the CL spectrum of 3 and 4 nm particles of CdSe coated with ZnS was previously reported and attributed to the quantum-confined Stark effect.<sup>47</sup>

CL spectra of the *annealed* nanoparticles (525 °C) and the Sarnoff phosphor are also shown in Fig. 6. The CL from these samples appeared yellow to the eye, suggesting that the charging problem described above was eliminated, perhaps by the increased particle size. The emission spectrum of the annealed nanoparticles was, however, slightly redder than the commercial phosphor. The peak wavelength of the annealed nanoparticles was 582 nm, compared to 580 nm for the Sarnoff. The Commission Internationale de l'Éclairage 1931 color coordinates were  $(x,y)=(0.526,0.472)$  and  $(0.522, 0.475)$ , respectively. The difference in color may be a result of the different crystal structures, as discussed in Sec. III C 1. The nanophosphor contains a mixture of the zincblende and wurtzite structures, while the Sarnoff is entirely wurtzite.

The annealed nanophosphors were approximately 200 times brighter than the unannealed particles and 40% as bright as the Sarnoff phosphor (electron beam voltages between 650 and 3150 V and currents in the range of 25–40  $\mu$ A). Figure 8 shows a plot of the luminance as a function of voltage. In addition, the annealed nanoparticles exhibited 50% less saturation as the electron-beam current density was increased from 5 to 100  $\mu$ A/cm<sup>2</sup> (1150 V). Details of these measurements have been published elsewhere.<sup>6</sup> We note that the tan color of the powder and the very poor PL efficiency

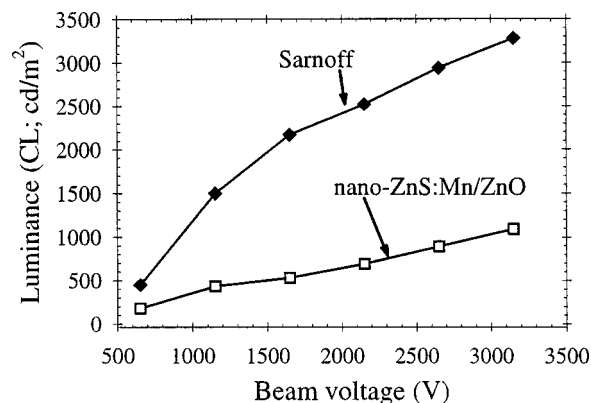


FIG. 8. Plot of the CL vs electron-beam acceleration voltage for ZnO-capped ZnS:Mn nanoparticles annealed at 525 °C (open squares) and the Sarnoff commercial phosphor (filled diamonds). The mean particle sizes are 100 nm and 4  $\mu$ m, respectively. The average crystallite sizes are 20 and 32 nm. The annealed nanoparticles are approximately 40% as bright as the commercial phosphor.

indicate that there were probably still some impurities in the sample. Removal of these impurities should further increase the phosphor's brightness.

The ZnO cap layer was essential for bright CL. Samples that were capped with MgO were only 25% as bright after annealing at 525 °C. Samples with no inorganic cap were substantially dimmer. As mentioned above, the MgO-capped and uncapped samples were dark gray in color after annealing, which certainly reduces the light-emitting efficiency. It appears, therefore, that the ZnO capping layer plays an important (but not understood) role during the annealing process.

Varying the concentration of the Mn ions within the ZnS lattice might also increase the brightness of the emission from the phosphor. The precursor MnCl<sub>2</sub> concentration of 0.7 mol % optimized the PL brightness,<sup>26</sup> but might not be optimal for CL. Among the unannealed phosphors, we observed an increase in CL brightness when the concentration of precursor MnCl<sub>2</sub> was increased to 1.4 mol %. These samples, however, have not been annealed.

#### IV. SUMMARY AND CONCLUSION

We have annealed ZnS:Mn nanoparticles in vacuum and have measured the sizes of the particles and crystallites, the lattice parameters and structure of the ZnS host, and the local environment around the Mn ions. The 3.5 nm unannealed particles exhibited a tetragonal distortion of the ZnS lattice and a reduced Mn–S bond length. The EPR spectra suggested that the Mn ions reside at or near the particle surface, as would be expected in such small particles. The EXAFS spectra indicated fewer than four nearest S neighbors around the Mn, which is consistent with the Mn residing near the particle surface. We observed a blueshift of the PL excitation spectrum in the unannealed samples because of the quantum confinement effect. The emission from the Mn ions, however, did not depend significantly on the particle size (in contradiction of previous reports). Annealing at temperatures

up to 350 °C did not significantly reduce the lattice distortion, but did cause growth of some of the particles and an increase of the average crystallite size.

Annealing at 400 °C or higher caused relaxation of the lattice distortion and (partial) conversion of the ZnS structure to wurtzite. This transition occurred at a temperature approximately 600 °C less than the corresponding point for bulk ZnS (1020 °C). Reduction of the *melting* temperature of nanoparticles has been observed and explained by considering surface tension (see Ref. 3 and references within) or surface phonons,<sup>4,48,49</sup> and a similar analysis might account for the reduced solid-solid phase transition temperature. A thermodynamic instability caused by a large surface energy might also explain why the size of the particles increases dramatically, coincident with the phase change. It is not clear, however, how the particle growth, phase change, and relaxation of the lattice distortion are related.

The length of the Mn–S bond reveals an interesting phenomenon. After annealing at 525 °C, the particle and/or crystallite size was large enough to relax the strain in the ZnS lattice (from XRD), yet the Mn–S bond length remained 0.6% ± 0.2% less than the bulk value (from EXAFS). In an earlier XAFS study, Soo *et al.*<sup>42</sup> observed a size dependence of the Mn–S bond length and Mn valency. Apparently the Mn valency (hence, ionic radius and Mn–S bond length) is more sensitive to particle or crystallite size than the Zn valency (hence, Zn–S bond length and lattice parameter).

Looking at CL, we found that the *unannealed* particles were subject to strong charging, which caused a significant redshift of the emission. Some improvement was seen after annealing at 400 °C, perhaps due to the partial conversion to wurtzite. A substantial improvement after annealing at 525 °C is attributed to further conversion to wurtzite, or to increased Mn–Mn interactions inferred from the EPR spectra. A systematic survey of samples with different Mn concentrations should distinguish between these two causes. The improvement in luminescence is not attributable to the average crystallite size, which did not change significantly upon increasing annealing temperature from 400 to 525 °C. The cathodoluminescent efficiency of the phosphor made from nanoparticles was within 40% of that of the commercial Sarnoff phosphor.<sup>6</sup>

Finally, we noted that addition of ZnO cap to the nanoparticles substantially increased the CL. The dark gray color of the particles that were uncapped or capped with MgO suggests that the ZnO cap layer might help maintain the stoichiometry while annealing in vacuum. This would be an interesting area for further study.

## ACKNOWLEDGMENTS

The authors gratefully acknowledge Mike Smith, Gary Rubin, Yongchi Tian, Ron Price, and Charles Dulcey for their valuable contributions.

<sup>1</sup>L. E. Brus, *J. Chem. Phys.* **80**, 4403 (1984).

<sup>2</sup>J. H. Davies, *The Physics of Low-Dimensional Semiconductors* (Cambridge University Press, Cambridge, UK, 1998).

<sup>3</sup>A. N. Goldstein, C. M. Echer, and A. P. Alivisatos, *Science* **356**, 1425 (1992).

<sup>4</sup>K. Hoshino and S. Shimamura, *Philos. Mag.* **A 40**, 137 (1979).

<sup>5</sup>S. B. Qadri, E. F. Skelton, D. Hsu, A. D. Dinsmore, J. Yang, H. F. Gray, and B. R. Ratna, *Phys. Rev. B* **60**, 9191 (1999).

<sup>6</sup>A. D. Dinsmore, D. S. Hsu, H. F. Gray, S. B. Qadri, Y. Tian, and B. R. Ratna, *Appl. Phys. Lett.* **75**, 802 (1999).

<sup>7</sup>C.-C. Chen, A. B. Herhold, C. S. Johnson, and A. P. Alivisatos, *Science* **276**, 398 (1997).

<sup>8</sup>S. H. Tolbert, A. B. Herhold, L. E. Brus, and A. P. Alivisatos, *Phys. Rev. Lett.* **76**, 4384 (1996).

<sup>9</sup>Y. L. Soo, S. W. Huang, Y. H. Kao, V. Chhabra, B. Kulkarni, J. V. D. Veladias, and R. N. Bhargava, *Appl. Phys. Lett.* **75**, 2464 (1999).

<sup>10</sup>E. T. Goldburt, B. Kulkarni, R. N. Bhargava, J. Taylor, and M. Libera, *J. Lumin.* **72–74**, 190 (1997).

<sup>11</sup>B. M. Tissue, *Chem. Mater.* **10**, 2837 (1998).

<sup>12</sup>A. Konrad, T. Fries, A. Gahn, F. Kummer, U. Herr, R. Tidecks, and K. Samwer, *J. Appl. Phys.* **86**, 3129 (1999).

<sup>13</sup>D. K. Williams, B. Bihari, B. M. Tissue, and J. H. McHale, *J. Phys. Chem. B* **102**, 916 (1998).

<sup>14</sup>H. Meyssamy, K. Riwozky, A. Kornowski, S. Naused, and M. Haase, *Adv. Mater.* **11**, 840 (1999).

<sup>15</sup>G. Counio, S. Esnouf, T. Gacoin, and J. P. Boilot, *J. Phys. Chem.* **100**, 20021 (1996).

<sup>16</sup>K. Yanata, K. Suzuki, and Y. Oka, *J. Appl. Phys.* **73**, 4595 (1993).

<sup>17</sup>L. D. Sun, C. H. Liu, C. S. Liao, and C. H. Yan, *J. Mater. Chem.* **9**, 1655 (1999).

<sup>18</sup>R. N. Bhargava, D. Gallagher, and T. Welker, *J. Lumin.* **60 & 61**, 275 (1994).

<sup>19</sup>Y. Wang, N. Herron, K. Moller, and T. Bein, *Solid State Commun.* **77**, 33 (1991).

<sup>20</sup>R. N. Bhargava, D. Gallagher, X. Hong, and A. Nurmikko, *Phys. Rev. Lett.* **72**, 416 (1994).

<sup>21</sup>K. Sooklal, B. S. Cullum, S. M. Angel, and C. J. Murphy, *J. Phys. Chem.* **100**, 4551 (1996).

<sup>22</sup>C. Jin, J. Yu, L. Sun, K. Dou, S. Hou, J. Zhao, Y. Chen, and S. Huang, *J. Lumin.* **66 & 67**, 315 (1996).

<sup>23</sup>H. Yang, Z. Wang, L. Song, M. Zhao, Y. Chen, K. Dou, J. Yu, and L. Wang, *Mater. Chem. Phys.* **47**, 249 (1997).

<sup>24</sup>T. Igarashi, T. Isobe, and M. Senna, *Phys. Rev. B* **56**, 6444 (1997).

<sup>25</sup>L. M. Gan, B. Liu, C. H. Chew, S. J. Xu, S. J. Chua, G. L. Choy, and G. Q. Xu, *Langmuir* **13**, 6427 (1997).

<sup>26</sup>J. P. Yang, H. Gray, D. Hsu, S. B. Qadri, G. Rubin, B. R. Ratna, W. L. Warren, and C. H. Seager, *J. Soc. Inf. Disp.* **6**, 139 (1998).

<sup>27</sup>U. Soehling, G. Jung, D. U. Saenger, S. Lu, B. Kutsch, and M. Mennig, *J. Sol-Gel Sci. Technol.* **13**, 685 (1998).

<sup>28</sup>J. Yu, H. Liu, Y. Wang, and W. Jia, *J. Lumin.* **79**, 191 (1998).

<sup>29</sup>J. Yu, H. Liu, Y. Wang, F. E. Fernandez, and W. Jia, *J. Lumin.* **76–77**, 252 (1998).

<sup>30</sup>A. A. Bol and A. Meijerink, *Phys. Rev. B* **58**, R15997 (1998).

<sup>31</sup>S. J. Xu, S. J. Chua, B. Liu, M. Gan, C. H. Chew, and G. Q. Xu, *Appl. Phys. Lett.* **73**, 478 (1998).

<sup>32</sup>D. Denzler, M. Olschewski, and K. Sattler, *J. Appl. Phys.* **84**, 2841 (1998).

<sup>33</sup>S. Puvvada, S. Baral, G. M. Chow, S. B. Qadri, and B. R. Ratna, *J. Am. Chem. Soc.* **116**, 2135 (1994).

<sup>34</sup>J. P. Yang, S. B. Qadri, and B. R. Ratna, *J. Phys. Chem. B* **100**, 17255 (1996).

<sup>35</sup>T. A. Kennedy, E. R. Glaser, P. B. Klein, and R. N. Bhargava, *Phys. Rev. B* **52**, R14356 (1995).

<sup>36</sup>M. Newville, B. Ravel, D. Haskel, E. A. Stern, and Y. Yacoby, *Physica B* **208–209**, 154 (1995).

<sup>37</sup>H. McMurdie, E. Evans, B. Paretzkin, W. Wong-Ng, and L. Ettinger, *Powder Diffr.* **1**, 77 (1986).

<sup>38</sup>T. Teranishi and M. Miyake, *Chem. Mater.* **10**, 594 (1998).

<sup>39</sup>J. E. Lennard-Jones, *Z. Kristallogr.* **75**, 215 (1930).

<sup>40</sup>H. W. Leverenz, *An Introduction to Luminescence of Solids* (Wiley, New York, 1950).

<sup>41</sup>*Phosphor Handbook*, edited by S. Shionoya and W. M. Yen (Chemical Rubber Corp., Boca Raton, FL, 1999).

<sup>42</sup>Y. L. Soo, Z. H. Ming, S. W. Huang, Y. H. Kao, R. N. Bhargava, and D. Gallagher, *Phys. Rev. B* **50**, 7602 (1994).

<sup>43</sup>H. E. Gumlich, *J. Lumin.* **23**, 73 (1981).

<sup>44</sup>W. Busse, H. E. Gumlich, B. Meissner, and D. Theis, *J. Lumin.* **12**, 693 (1976).

- <sup>45</sup>D. Gallagher, W. E. Heady, J. M. Racz, and R. N. Bhargava, *J. Mater. Res.* **10**, 870 (1995).
- <sup>46</sup>R. Rossetti, R. Hull, J. M. Gibson, and L. E. Brus, *J. Chem. Phys.* **82**, 552 (1985).
- <sup>47</sup>J. Rodriguez-Viejo, K. F. Jensen, H. Mattoussi, J. Michel, B. O. Dabbousi, and M. G. Bawendi, *Appl. Phys. Lett.* **70**, 2132 (1997).
- <sup>48</sup>M. Wautelet, *J. Phys. D* **24**, 343 (1991).
- <sup>49</sup>P. R. Couchman and C. L. Ryan, *Philos. Mag. A* **37**, 369 (1978).